Journal of Magnetic Resonance **149,** 144–148 (2001)
doi:10.1006/jmre.2000.2283, available online at http://www.idealibrary.com on IDEAL®

Dynamic NMR Microscopy of Gas Phase Poiseuille Flow

Lana G. Kaiser, John W. Logan, Thomas Meersmann,[1] and Alexander Pines[2]

Materials Sciences Division, Lawrence Berkeley National Laboratory, and Department of Chemistry, University of California at Berkeley, Berkeley, California 94720

Received September 22, 2000; revised December 19, 2000

Dynamic NMR microscopy has been used to study xenon gas undergoing Poiseuille flow in the regime where deterministic and stochastic motions are the same order of magnitude. For short observation time, the flow profile images are largely influenced by the longitudinal diffusion, manifested by large displacements in both positive and negative directions. For longer observation time, the effect of the mixing between the fast and slow flow components due to transverse diffusion becomes apparent. A spin-echo version of the dynamic NMR experiment yields images exhibiting strong distortions for longer observation time due to fast diffusion under the "natural" gradient from magnetic field inhomogeneity (compared to results obtained with a stimulated echo version). This effect is used as an edge-enhancement filter by employing a longer time duration of the imaging gradient in a stimulated echo experiment.

Key Words: **Poiseuille flow; xenon NMR; gas phase NMR; Taylor dispersion; gas flow.**

INTRODUCTION

Fluid transport is an important phenomenon studied in a wide number of disciplines ranging from statistical mechanics to chemical engineering. One of the most intriguing aspects of those studies is the interplay between deterministic and stochastic molecular displacements arising, respectively, from coherent flow and Brownian motion. This problem was studied in detail by Taylor (*1*) and Aris (*2*) for the case of a fluid flowing through a cylindrical pipe, where viscosity shear imposes a parabolic distribution of molecular displacements, separating the entire ensemble into velocity streamlines with the smallest displacement at the walls of the pipe and the largest displacements in the center. The increase in effective diffusion that arises from molecules randomly sampling streamlines with different velocities is referred to as "Taylor dispersion." The complete expression for the effective diffusion, under laminar flow conditions, has been derived by Van den Broeck (*3*) for both short ($t \ll a^2/D$) time scales,

$$D^* = D + \frac{1}{6}V_{\text{ave}}^2 t + \frac{4}{3}DV_{\text{ave}}^2 t^2/a^2 + \cdots, \qquad [1]$$

and long ($t \gg a^2/D$) time scales,

$$D^* = D + \frac{V_{\text{ave}}^2 a^2}{48D}, \qquad [2]$$

where D^* is the effective diffusion coefficient (or dispersion coefficient in this case), D is the self-diffusion coefficient, V_{ave} is the average fluid velocity, a is a pipe radius, and t is the time used to measure longitudinal displacement. Equation [2] represents an asymptotic regime where the dispersion coefficient becomes time-independent due to full sampling of all the velocities by diffusive motion. For typical liquids undergoing the Poiseuille flow, coherent motion has an enormous influence on the effective diffusion coefficient measured by standard pulsed field gradient (PFG) NMR, rendering contributions from the purely stochastic term negligible. Recent experiments (*4*) have verified the preasymptotic dispersion theory for such a system by measuring the longitudinal displacements of liquid octane molecules undergoing Poiseuille flow using PFG NMR. A gradual transition of the probability propagator from Poiseuille flow to Taylor–Aris dispersion was investigated by varying the observation time.

The time-dependent behavior of the displacement probability propagator can be very different for gas phase Poiseuille flow, where large stochastic displacements are often comparable to those arising from coherent motion. In this Communication, we present an experimental study of gas phase Poiseuille flow in such a regime via ^{129}Xe dynamic NMR microscopy. Xenon gas has a self-diffusion coefficient of 5.5 mm^2/s at 1 atm; the displacements due to diffusion and flow are, respectively, $\sqrt{2Dt}$ and Vt. Thus, for gas phase xenon undergoing Poiseuille flow with an average velocity ca. 20 mm/s, displacements from coherent and stochastic motion are of the same order of magnitude.

PFG NMR is an established technique, capable of monitoring both flow and diffusion for a wide range of temporal and spatial scales (*5–7*). Dynamic NMR microscopy is an extension of the PFG method, where displacement encoding can be combined with spatial encoding with subsequent reconstruction of velocity

[1] Permanent address: Department of Chemistry, Colorado State University, Fort Collins, CO 80235.

[2] To whom correspondence should be addressed. E-mail: pines@cchem.berkeley.edu.

1090-7807/01 $35.00

and diffusion maps (*8*). In order to overcome the severe insensitivity of gas phase NMR, a continuous flow optical pumping system (*9*) has been employed. This system provides sufficient signal to perform 2D and 3D gas phase NMR microscopy experiments with 100-μm resolution in three dimensions, with signal intensities comparable to those in liquid ^{1}H NMR (*10*). In the present study, laser-polarization of xenon under continuous flow conditions produces an enhancement in nuclear polarization of ca. 4 orders of magnitude, greatly facilitating the experimental implementation of gas phase NMR microscopy.

MATERIALS AND METHODS

All experiments were performed on a Chemagnetics/Varian Infinity spectrometer at a magnetic field of 4.3 T, corresponding to a ^{129}Xe frequency of 49.5 MHz. The homebuilt probe with a commercial microimaging gradient set contains a glass pipe (id = 4 mm) attached via Teflon tubing to the optical pumping apparatus described previously (*10*).

Figure 1A shows a stimulated echo version of the dynamic NMR microscopy experiment employed in this study, which uses a displacement encoding gradient in the flow direction (g_x) and spatial encoding gradient (G_y) in a direction perpendicular to the flow. The displacement of the spins during the period, Δ, between the gradient pulses, g, of duration, δ, results in a modification of the observed echo signal. The observed signal is given by

$$E(\mathbf{q}) = \exp[i2\pi\Delta V_{\text{ave}}\mathbf{q} - 4\pi^2 D(\Delta - \delta/3)q^2], \qquad [3]$$

where $\mathbf{q} = (2\pi)^{-1}\gamma\mathbf{g}\delta$ (*8*). Spatially resolved information is acquired by applying a frequency-encoding gradient (G_y) in a direction perpendicular to the flow. Following a 2D Fourier transform (FT), displacement profiles with the spin density averaged over the z-direction are obtained (the spatial dimension also could be processed using a Hankel transform or FT followed by an inverse Abel transform to fully utilize the cylindrical symmetry of the pipe (*11*)). Velocity profiles are constructed simply by dividing the displacement by the observation time, Δ. Thus, the expressions "displacement profiles" and "velocity profiles" are used interchangeably in this contribution.

The simulations are performed using Eq. [3] for an ensemble of $N_{\text{spins}} = 10^4$, with corrections for spins that flow out of the pipe during the observation time. For short Δ, D^* was approximated by D in the simulations. The data processing for the simulations and the experimental data are identical.

RESULTS AND DISCUSSION

Temporal Regimes of Gas Phase Poiseuille Flow in a Pipe

It is instructive to compare the displacement profile images for liquid pipe flow (where diffusion is only a small perturbation at time $\Delta < a^2/D$) and gas pipe flow. Figures 1B and 1C show a numerical simulation and experimental data, respectively, of the 2D dynamic NMR microscopy experiment for water flowing in a pipe (observation time, $\Delta = 20$ ms). The classical Poiseuille velocity profile along the cylindrical axis of a pipe is described by

$$V(r) = V_{\max}(1 - r^2/a^2), \qquad [4]$$

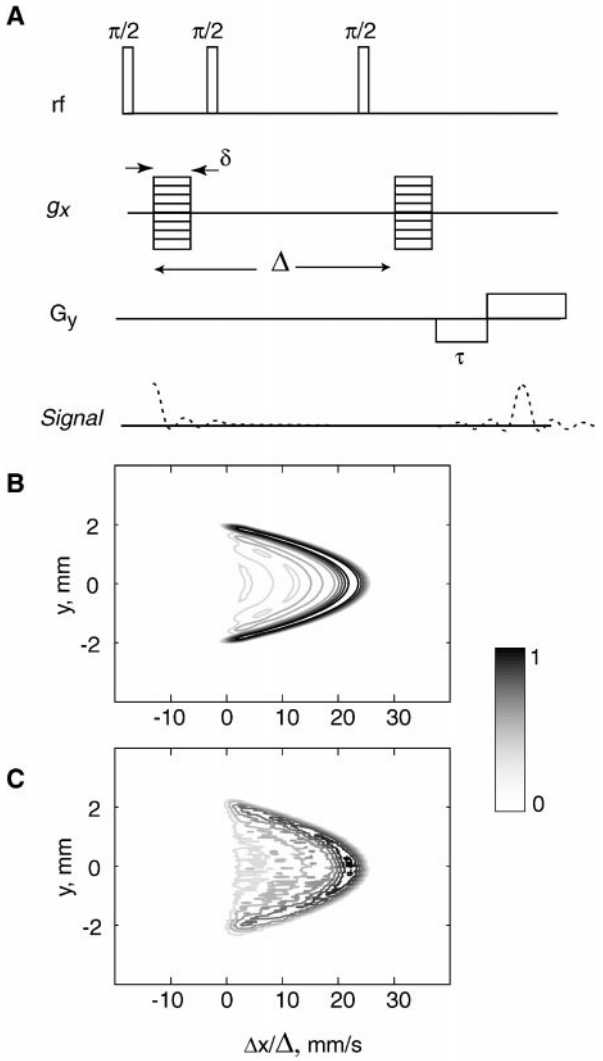

FIG. 1. A. Stimulated echo dynamic NMR microscopy pulse sequence. The first gradient pulse (g_x) of duration δ serves to encode the spatial positions of spins and the second gradient pulse has the effect of refocusing the magnetization. Molecular displacements (during time Δ) due to stochastic motion attenuate the amplitude, while coherent motion due to flow imposes a net phase shift on the observed signal. A second imaging gradient (G_y) is added in order to obtain a spatial map of displacements. A notable feature of the stimulated echo version is that during the displacement period, Δ, the magnetization is stored along the z-axis and is subject only to longitudinal relaxation. Bulk xenon gas has a sufficiently long T_1 that observation of the displacement is limited only by the spins flowing out of the detection region. B. Computer simulation of the joint spatial-velocity profile for water undergoing Poiseuille flow in a pipe (id = 4 mm, $D_{\text{water}} = 2.2 \times 10^{-3}$ mm^2/s, $V_{\text{ave}} = 11.5$ mm/s, $\Delta = 20$ ms). The stimulated echo pulse sequence of A is used to record 256×32 data sets with subsequent zero-filling to 512×256 points followed by 2D FFT. C. Experimental data with the same parameters as in B.

where

$$V_{\max} = \Delta P a^2 / 4\eta l \qquad [5]$$

and ΔP is the pressure decrease over the length l of the pipe, η is the dynamic viscosity, and a is the radius of the pipe. The average velocity of water as determined by volumetric analysis, 11.5 mm/s, is in good agreement with the extracted experimental average velocity, $V_{\max}/2 = 11.8$ mm/s. The nonzero signal intensity inside the parabola in the image is a result of spatial averaging of the spin density along the z-dimension (i.e., a consequence of recording only one spatial dimension). Figure 2 shows a numerical simulation (A) and experimental (B) flow profiles of xenon gas at 1.3 atm ($D = 4.5$ mm^2/s, $V_{\text{ave}} = 20$ mm/s). Gas phase profiles reflect large displacements due to longitudinal diffusion and, as a result, it is necessary to extract the maximum velocity value from the maximum of the Gaussian curves according to the procedure described in Ref. (*8*). This method is general and works for all fluids; however, in liquid flow, the velocity distribution in the longitudinal direction is sufficiently small so that an estimate of the maximum velocity can be made simply by the location of the parabola top in the displacement image (compare Figs. 1B and 2B). Another difference between profiles in Figs. 1B and 2B is the large negative displacement of xenon gas for short observation times (also a consequence of longitudinal diffusion).

A prominent feature of Fig. 2 is the temporal progression of the molecular displacements. Naively, we can identify two competing processes affecting the apparent velocity profiles, namely the longitudinal and transverse diffusion. In the short time limit, the displacements due to longitudinal diffusion are dominant. Here, one would expect to see a very broad distribution of apparent velocities. In the long time limit, transverse diffusion "blurs" the radial dependence of the velocity. The particles are able to sample the entire ensemble of the velocity streamlines across the pipe, thus flattening the parabolic distribution of velocities across the pipe compared to what is normally expected from Poiseuille flow. This behavior corresponds to the asymptotic limit of Eq. [2].

An estimate of the displacement due to flow and diffusion as a function of time is shown in Fig. 3A. There are two distinct temporal regimes; first, for short times, the behavior is determined by longitudinal diffusion ($t < 15$ ms); this situation is represented in Fig. 2B. Second, for longer times, the coherent displacements due to flow dominate as illustrated in Fig. 2C. The situation described in Fig. 3A does not include transverse stochastic displacements. Figure 2D ($\Delta = 130$ ms) shows the displacement profile image approaching the asymptotic regime, limited only by spin washout of the detection region.

The effective dispersion coefficients, D^*, have been obtained for the 2D data sets using the Stejskal–Tanner method as described elsewhere (*12*). The resulting D^* values are shown in Fig. 3B as function of Δ. An analytic expression for $D^*(\Delta)$ has been presented in (*12*):

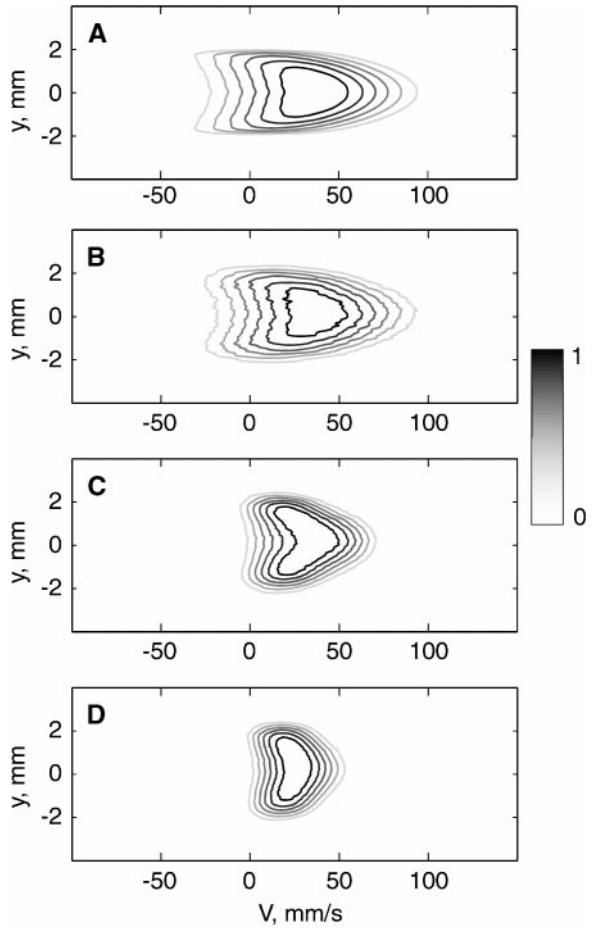

FIG. 2. Joint spatial-velocity images of xenon undergoing Poiseuille flow in a pipe (id = 4 mm, $D_{\text{Xe}} = 4.5$ mm^2/s, $V_{\text{ave}} = 20$ mm/s). Data sets of 256×32 points were collected using the stimulated echo pulse sequence depicted in Fig. 1A with subsequent zero-filling to 512×256 points followed by 2D FFT. Digital resolution in the spatial direction (y) is 100 μm. The velocity spectral window is kept constant in each of the images. A. Computer simulation ($\Delta = 10$ ms). B. Experiment ($\Delta = 10$ ms). C. Experiment ($\Delta = 60$ ms). D. Experiment ($\Delta = 130$ ms).

$$D^*(\Delta) = D + V_{\text{ave}}^2 \tau_c \left(1 + \frac{\tau_c}{\Delta}[\exp(-\Delta/\tau_c) - 1]\right), \qquad [6]$$

where τ_c is the correlation time of the velocity fluctuations. The experimental data points are correlated with Eq. [6], as indicated by the solid line in Fig. 3B. The velocity correlation time obtained from the line fitting, $\tau_c = 25$ ms, yields the dispersion coefficient in the asymptotic limit of $D^* = D + V_{\text{ave}}^2 \tau_c = 14$ mm^2/s.

Edge Enhancement Effect in Gas Phase Poiseuille Flow

The spin-echo version of the dynamic NMR experiment yields strongly distorted images for longer mixing times. Figures 4A–4C show displacement profile images of xenon at 0.8 atm

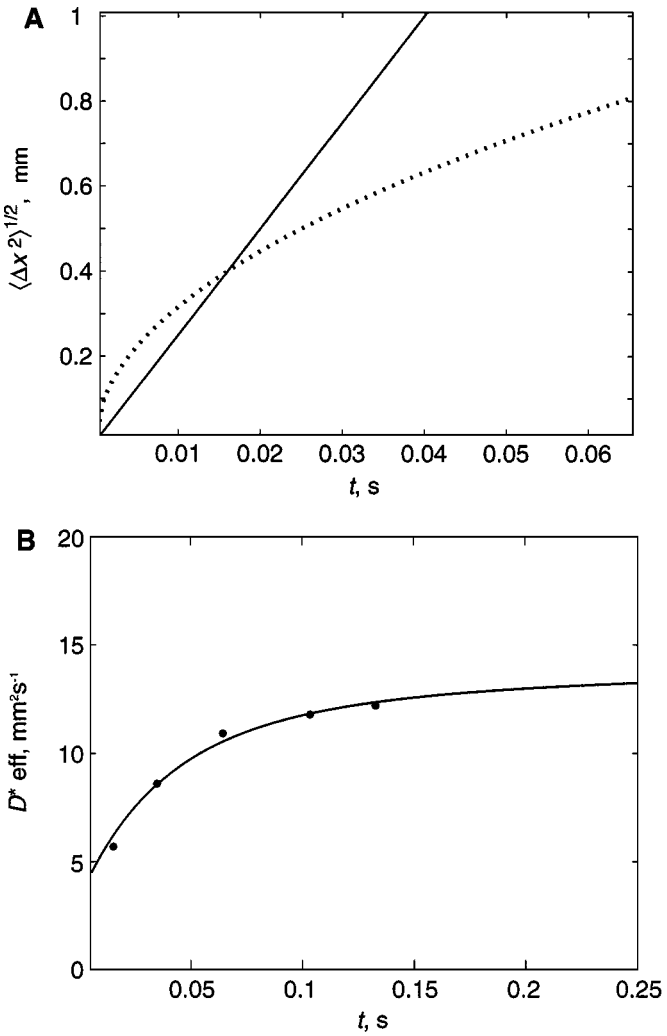

FIG. 3. A. Theoretical displacement due to velocity, $V_{ave}t$, and diffusion $\sqrt{2Dt}$ (dotted line) for the system described in Fig. 2 showing two distinct regimes for molecular displacements in this system; for short observation times, the molecular displacements are driven by stochastic process, and for longer observation times, the coherent displacements make a significant contribution. B. The effective dispersion coefficient as a function of observation time, Δ. The line represents the data fit to Eq. [6], approaching the asymptotic limit for long observation times. The dots correspond to the experimental effective dispersion coefficient for several different observation times.

(recorded with the spin-echo version of the PFG NMR microscopy experiment). For short observation time, the displacement profile of xenon in Fig. 4B is equivalent to the data in Fig. 2B; the slightly lower parabolic extension is due to the lower pressure of xenon gas. At longer measuring times such as in Fig. 4C ($\Delta = 100$ ms), the intensity in the middle is significantly lower, resulting in a pronounced image "hole" in the center of the pipe. The small "natural" gradient, always present in the magnetic field, can often be neglected in liquid and solid state time-dependent NMR studies. However, such a gradient can play a significant role in the image contrast in gas phase NMR. This effect is referred to as "edge enhancement," an increase of the rate of magnetization decay for higher diffusion in the presence of the magnetic field gradient (*13, 14*). Consequently, higher signal intensity persists at the edges where the diffusion is partially restricted. This effect can be exploited by imposing an imaging gradient so as to separate molecular displacements at the boundaries from those in the remainder of the system.

Indeed, it has been shown (*15*) that when an imaging gradient is applied for longer times (several milliseconds) in a xenon gas sample, only signal at the boundary remains. Figure 5 shows the application of the edge enhancement "filter" for gas phase Poiseuille flow. A stimulated echo pulse sequence (Fig. 1A), with a longer imaging gradient encoding time ($\tau = 5$ ms), is used to select spins at the boundaries, with the displacement spectral window, **q**, maintained constant. Figure 5A ($\Delta =$ 3 ms) demonstrates a nearly symmetric displacement distribution about $\Delta x = 0$ for the particles at the walls, corresponding to a very small flow contribution. On the other hand, the presence of unidirectional flow for $\Delta = 30$ ms (Fig. 5B) is significant.

Such an edge enhancement filter may be inserted in any period of the pulse sequence. When the filter occurs at the beginning of the pulse sequence, it might be possible to monitor the exchange between the slow and fast components, for example, the

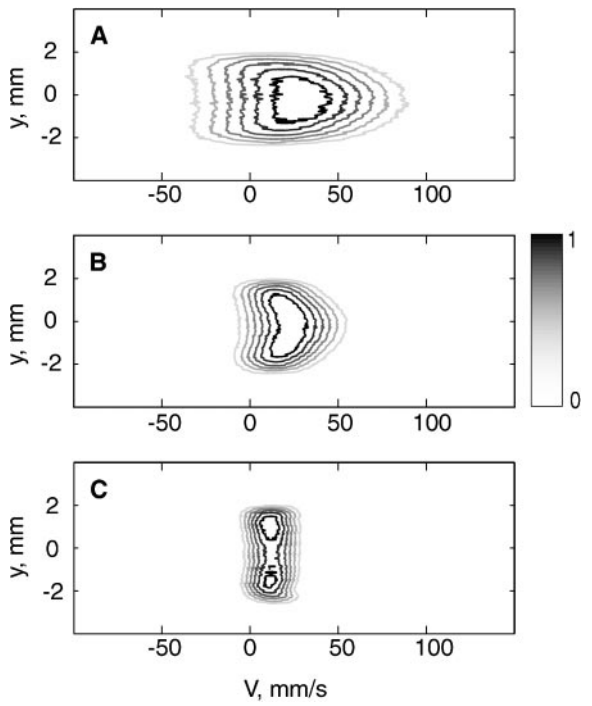

FIG. 4. Poiseuille pipe flow displacement profiles ($V_{ave} = 20$ mm/s) for xenon at 0.8 atm recorded using a spin-echo version of the dynamic NMR microscopy pulse sequence. A. Experimental data for $\Delta = 10$ ms. B. Experimental data for $\Delta = 50$ ms. C. Experimental data for $\Delta = 100$ ms. The reduced signal intensity in the middle of the pipe is a consequence of the edge enhancement effect induced by large random displacements under the natural inhomogeneity gradient of the magnet.

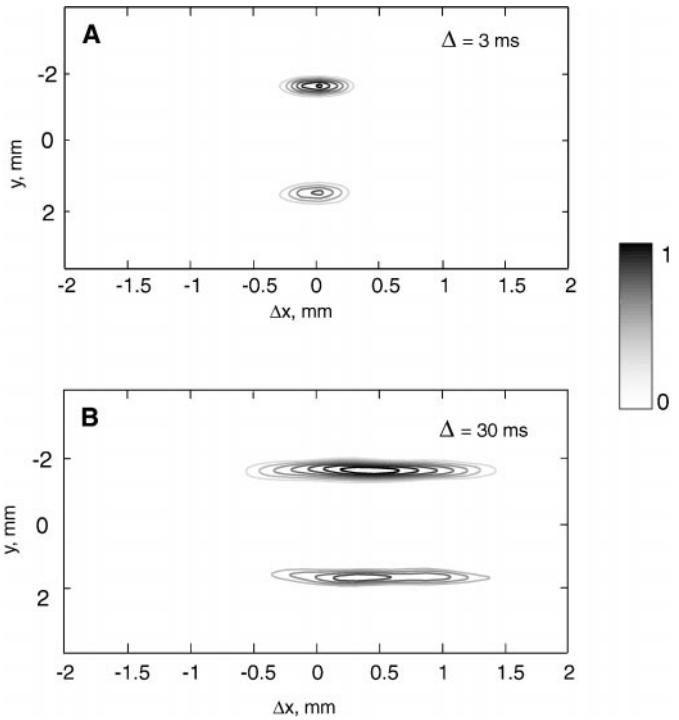

FIG. 5. Poiseuille flow displacement profiles ($V_{ave} = 27$ mm/s, $D = 8$ mm^2/s) for xenon at 0.7 atm recorded with the stimulated echo pulse sequence of Fig. 1A. Only particles at the walls are selected by the edge enhancement "filter." A modified imaging gradient time duration ($\tau = 5$ ms) was used. Data sets of 512×16 data points were collected. The data sets were 2D FFT after zero-filling to 1024×32 points. Digital resolution in spatial direction (y) is 100 μm. A. Displacement time, $\Delta = 3$ ms. B. Displacement time, $\Delta = 30$ ms.

appearance of spins at the center of the pipe for longer Δ. The same method could be applied in gas phase dynamic NMR studies of any system with restricted diffusion (e.g., porous media) in order to observe dynamic interchange between the boundaries and the bulk.

We have presented a dynamic NMR microscopy study of gas phase Poiseuille flow with large stochastic displacements in different temporal regimes. The results indicate that longitudinal diffusion dominates the displacement profile for short observation times. The transverse diffusion influence is more apparent for longer observation times. Rapid self-diffusion of the gas necessitates a stimulated echo PFG experiment for long evolution times ($\Delta > 100$ ms). The continuous flow laser-polarized ^{129}Xe technique provides great versatility in preparing custom systems for studying transport phenomena (both diffusion and velocity can be varied by almost two orders of magnitude in our system). For example, in a system with average pore size of 1 mm, it is possible to monitor displacements via dynamic NMR microscopy for Peclet numbers ranging from 1 to ca. 1000 by adjusting flow rates and gas pressure. In the future, it would be interesting to investigate in detail the onset of the turbulence in xenon gas pipe flow (*16*) and the use of the edge enhancement filter for monitoring dynamic interchange between the boundaries and the bulk of porous media.

ACKNOWLEDGMENTS

The authors thank Professor P. T. Callaghan for helpful discussions. This work was supported by the Director, Office of Energy Research, Office of Basic Energy Science, Materials Sciences Division, of the U. S. Department of Energy under Contract DE-AC03-76SF00098. TM thanks the Alexander von Humboldt Foundation for a Feodor-Lynen Fellowship.

REFERENCES

1. G. I. Taylor, *Proc. Roy. Soc. London A* **219,** 186–203 (1953).
2. R. Aris, *Proc. Roy. Soc. London A* **235,** 67–77 (1956).
3. C. Van den Broeck, *Phys. A* **112A,** 343–352 (1982).
4. S. L. Codd, B. Manz, J. D. Seymour, and P. T. Callaghan, *Phys. Rev. E* **60,** R3491–R3494 (1999).
5. K. J. Packer and J. J. Tessier, *Mol. Phys.* **87,** 267–272 (1996).
6. J. Karger and W. Heink, *J. Magn. Reson.* **51,** 1–7 (1983).
7. D. O. Kuethe and J.-H. Gao, *Phys. Rev. E* **51,** 3252–3262 (1995).
8. P. T. Callaghan, "Principles of Nuclear Magnetic Resonance Microscopy," Oxford Univ. Press, New York (1991).
9. E. Brunner, M. Haake, L. Kaiser, J. Reimer, and A. Pines, *J. Magn. Reson.* **138,** 155–159 (1999), doi:10.1006/jmre.1998.1675.
10. L. G. Kaiser, T. Meersmann, J. W. Logan, and A. Pines, *Proc. Natl. Acad. Sci. USA* **97,** 2414–2418 (2000).
11. P. D. Majors and A. Caprihan, *J. Magn. Reson.* **94,** 225–233 (1991).
12. J. D. Seymour and P. T. Callaghan, *AIChE. J.* **43,** 2096–2111 (1997).
13. B. Putz, D. Barsky, and K. Schulten, *J. Magn. Reson.* **97,** 27–53 (1992).
14. P. Callaghan, A. Coy, L. C. Forde, and C. J. Rofe, *J. Magn. Reson. A* **101,** 347–350 (1993).
15. Y.-Q. Song, B. M. Goodson, B. Sheridan, T. M. de Swiet, and A. Pines, *J. Chem. Phys.* **108,** 6233–6239 (1998).
16. L. G. Kaiser, Ph.D. dissertation, University of California, Berkeley (2000).